SEISMIC RESPONSE OF RIGID CYLINDRICAL CAISSONS EMBEDDED IN INHOMOGENEOUS SOIL STRATA

by

Aggelos Tsikas[1], George Anoyatis[2], Stijn François[3], George Gazetas[4]

[1]Quantum Neural Technologies (QNT), Athens, Greece

[2]KU Leuven, Department of Civil Engineering, Hydraulics and Geotechnics Section, Bruges, Belgium

[3]KU Leuven, Department of Civil Engineering, Structural Mechanics Section, Leuven, Belgium

[4]National Technical University of Athens (NTUA), School of Civil Engineering, Department of Geotechnical Engineering, Athens, Greece

Abstract. This study develops a novel reference analytical elastodynamic model for the harmonic and seismic response of a rigid caisson, extending the pioneering work of Veletsos & Younan (1994) to vertically inhomogeneous soils. Both the caisson and the soil stratum are supported on a non-deformable base which is subjected to uniform horizontal motion. The solution is based on Sturm-Liouville's theory and Helmholtz's decomposition and makes use of the realistic simplifying assumption of universally vanishing the vertical normal stresses in the soil medium. An extensive parametric analysis in terms of horizontal soil pressures, shear force and bending moment for a soil shear modulus which increases with depth, demonstrating the effect of the type and degree of soil inhomogeneity on the caisson's response. The findings offer an improved understanding of soil-caisson interaction mechanism in presence of inhomogeneous soils, which can be used to validate numerical models and interpret results for more complex systems.

Key words: dynamic soil-structure interaction, analytical model, elastodynamics, soil inhomogeneity, rigid caisson, seismic response, Fourier series expansion, Sturm-Liouville theory.

INTRODUCTION

Cylindrical caissons are used frequently as foundations for bridge piers and towers, as vertical shafts for a variety of underground structures such as ventilation and escape routes for tunnels, as embedded storage tanks and vaults, and as deeply embedded foundations for special structures. Their seismic response has received rather indirect attention, in the form of research on the dynamic impedances and seismic response of embedded foundations (e.g., Tajimi 1969, 3. Beredugo & Novak 1972, Day & Frazier 1979, Domingue 1978, Tassoulas & Kausel 1983, Wolf & Somaini 1986, Gazetas & Tassoulas 1987, Apsel & Luco 1987, Luco & Wong 1987, Pais & Kausel 1988). In the past couple decades, there is a sequence of papers by Gerolymos and Gazetas dealing with the lateral response of circular, square and rectangular shaped rigid caissons under inertial and kinematic loading, which include the development of a Winkler model for the dynamic response of a caisson embedded in an elastic half-space subjected to inertial and kinematic seismic loading (Gerolymos & Gazetas 2006a), .the subsequent development of a most general inelastic Winkler model to account for the effects of soil and interface nonlinearities in the response of a caisson subjected to strong static or dynamic excitation (Gerolymos & Gazetas 2006b), and a final study on the validation of the proposed nonlinear method through comparisons with3D-finite element analysis, and scaled lateral load tests (Gerolymos & Gazetas 2006c). In the framework of Winkler formulations, Varun et al. (2009) developed an analytical model for the prediction of the response of rigid cylindrical caisson foundations embedded in linear elastic soil media, providing analytical expressions for the transfer functions of kinematic interaction effects, and for the prediction of forced vibration and seismic transient response. Additional studies investigate the dynamic response of suction caissons in visco-elastic soils using finite element models (e.g., Latini & Zania 2017). Among the few published theoretical studies specifically addressing the caisson under seismic excitation we mention the work of Harada et al. (1981, 1985), Guan & Novak (1994), Veletsos & Younan (1994, 1998), Saitoh (2001), Assimaki et al. (2001).

The work presented in this paper is an extension of the rigorous analytical model described in the studies of Veletsos & Younan (1994b, 1998), which investigate the dynamic soil pressures that develop on the vertical surface of a cylindrical "vault" embedded in a homogeneous soil stratum. Both the visco-elastic soil stratum and the rigid caisson were considered fixed on a rigid base (bedrock), which is a realistic idealization for many caisson foundations of large bridge piers. The assumption of vanishing vertical stresses was a key assumption introduced by Veletsos & Younan (1994b), demonstrating the superiority of the model over the more restrictive approach of vanishing vertical displacements proposed by Tajimi (1969), which resulted in a stiffer soil medium.

One of the key findings of Veletsos & Younan (1994b, 1998) refers to the distribution of normal and tangential stresses acting on the caisson surface. Both stresses increase from the base to the top, following an approximately parabolic distribution, with minimal dependence on the aspect ratio H/R (where H is the height and R is the radius of the vault). The low-frequency ("quasi-static") maximum

values of the resultant horizontal force along the circumference at the top of the caisson was found to be on the order of $3.7\,\pi\rho\ddot{u}_g RH$, for an aspect ratio of $H/R = 3$, where $\ddot{u}_g$ denotes the acceleration amplitude at the rigid base. However, such high alternating forces (±) near the ground surface are unlikely to develop, given the vanishingly small pre-existing ("geostatic") normal compressive stresses at shallow depths. These forces either exceed the frictional capacity of the interface or imply net tension. Such forces are unrealistic since they arise as a direct consequence of two fundamental assumptions: linear elasticity (Timoshenko 1987) and soil homogeneity (Menahem & Singh 1981).

This work relaxes the second of the aforementioned assumptions by treating the soil shear modulus as a function of depth, thereby accounting for the increase in soil stiffness (soil inhomogeneity) due to increasing confining pressure. As a result, the predicted distributions of soil reactions on the caisson wall no longer exhibit maxima at the top, aligning more closely with observed behavior. In addition to refining the soil-structure interaction model, a second objective of this research is to conduct a parametric analysis to investigate the "effective input motion" at the top of the caisson, which arises from capturing the kinematic interaction between caisson and the surrounding soil. This effective motion is critical for determining the appropriate input needed to evaluate the response of the superstructure. To achieve these objectives, an elegant solution is developed in the frequency domain. The treatment presented is relatively short, straightforward and novel, without relying on higher-level mathematics. The response of more complex types of embedded structures is beyond the scope of this work and has been developed in ongoing studies, which will be made available in forthcoming works.

SYSTEM CONSIDERED

The system examined is shown in Figure 1: the caisson is modelled as a rigid circular cylinder of radius R, is embedded in a soil layer of thickness H and infinite lateral extent, overlying a rigid base. The soil is defined by its constant material density ρ_s, Poisson's ration ν_s, and hysteretic material damping β_s, expressed through the complex valued soil shear modulus of elasticity $G_s^* = G_s(1 + 2i\beta_s)$. $G_s = G_s(z)$ varies with depth (z) according to a monotonically increasing function of depth i.e., $G = G_0\, f(z/H)$, G_0 being a reference modulus at the soil surface. Both the cylinder and the base of the layer are considered to undergo a rigid body horizontal harmonic acceleration $\ddot{u}_g(t) = \ddot{u}_g\, e^{i\omega t}$, of maximum amplitude $\ddot{u}_g$. The main objective is to evaluate the distribution of normal and shear stresses in the soil acting along the circumference of the caisson, as well as the resulting horizontal force per unit depth along its height.

METHOD OF ANALYSIS

The rationale for this analysis can be understood by first considering the far-field action of the soil medium, namely the response computed under the assumption that the layer is of infinite extend and that no caisson is present. Under these conditions, each vertical strip of the medium behaves as an independent cantilever shear beam. The resulting response, which is naturally independent of the horizontal position coordinate, constitutes the particular solution to the governing equation of motion for the medium.

The response of the considered system (Fig. 1), within the framework of linear elasticity (e.g., Timoshenko & Goodier 1987, Menahem & Singh 1981, Courant & Hilbert 1953), can be evaluated by superimposing the homogeneous solution (which represents free vibration of surrounding medium) onto the far-field particular solution. This approach accounts for the effect of the pressures exerted by the caisson. The magnitude and distribution of these pressures at any given time must be such that the resulting displacements, combined with those induced by the ground motion under free-field conditions, match the caisson displacements. The caisson pressures p, necessary to ensure compatibility of the displacements along the caisson, can be expressed as follows

$$p = \widetilde{K}\,(u_{ff} - u_c) \tag{1}$$

where $\widetilde{K}$ denotes a generalized impedance of the soil medium, u_{ff} is the free-field displacement relative to the base, and u_c is the corresponding displacement of the caisson. For the special case of a fixed-based rigid caisson, its relative displacement u_c equals to zero, and the caisson pressures are then simply proportional to the far-field motion. It should be noted that when the soil medium is of infinite extent, the boundary conditions at infinity become essentially radiation conditions. This implies that certain integrals vanish over the partial surface of spheres of infinite radius. The proposed approach can be modified to be valid in any orthogonal curvilinear coordinate system (Courant & Hilbert 1953).

With reference to the cylindrical system of coordinates shown in Figure 1, the equilibrium o forces acting on an arbitrary soil element in r, z, and θ generate the equations of motion of the medium (ignoring external forces) as follows

$$\frac{\partial \sigma_r}{\partial \xi} + \frac{1}{\xi}\frac{\partial \tau_{r\theta}}{\partial \theta} + \frac{R}{H}\frac{\partial \tau_{rz}}{\partial \eta} + \frac{1}{\xi}(\sigma_r - \sigma_\theta) = \rho_s R \frac{\partial^2 u}{\partial t^2} \tag{2a}$$

$$\frac{\partial \tau_{r\theta}}{\partial \xi} + \frac{1}{\xi}\frac{\partial \sigma_\theta}{\partial \theta} + \frac{R}{H}\frac{\partial \tau_{z\theta}}{\partial \eta} + \frac{2}{\xi}\tau_{r\theta} = \rho_s R \frac{\partial^2 v}{\partial t^2} \tag{2b}$$

$$\frac{\partial \tau_{rz}}{\partial \xi} + \frac{1}{\xi}\frac{\partial \tau_{\theta z}}{\partial \theta} + \frac{R}{H}\frac{\partial \sigma_z}{\partial \eta} + \frac{1}{\xi}\tau_{rz} = \rho_s R \frac{\partial^2 w}{\partial t^2} \quad (2c)$$

in which $\xi = r/R$ and $\eta = z/H$ are dimensionless position coordinates, σ_r, σ_θ, σ_z are the normal stresses at an arbitrary point in space and the time along the r, θ and z spatial coordinates, respectively; u, v, and w are the corresponding horizontal, tangential and vertical soil displacement components relative to the moving rigid base; and the stresses $\tau_{r\theta}$, τ_{rz}, $\tau_{\theta z}$ are the shear stresses in the r-θ, r-z, and θ-z planes, respectively.

Building upon the work of Veletsos & Younan (1994), this study also adopts the fundamental assumption that, under the horizontal excitation considered at the rigid base, no vertical normal stresses develop anywhere in the medium i.e., $\sigma_z = 0$. It is further assumed that the variation of the vertical displacements in the horizontal direction is negligible i.e., $\partial w/\partial \xi = 0$ and $\partial w/\partial \theta = 0$, as this does not introduce significant errors in the solutions and aligns with the physics of the problem . Thus, the three governing equations of the rigorous elasticity reduce to the following two (Tsikas 1995)

$$\frac{\partial \sigma_r}{\partial \xi} + \frac{1}{\xi}\frac{\partial \tau_{r\theta}}{\partial \theta} + \frac{R}{H}\frac{\partial \tau_{rz}}{\partial \eta} + \frac{1}{\xi}(\sigma_r - \sigma_\theta) = \rho_s R \frac{\partial^2 u}{\partial t^2} \quad (3a)$$

and

$$\frac{\partial \tau_{r\theta}}{\partial \xi} + \frac{1}{\xi}\frac{\partial \sigma_\theta}{\partial \theta} + \frac{R}{H}\frac{\partial \tau_{\theta z}}{\partial \eta} + \frac{2}{\xi}\tau_{r\theta} = \rho_s R \frac{\partial^2 v}{\partial t^2} \quad (3b)$$

where the stress components are related to the displacement components by (Veletsos & Younan, 1994)

$$\frac{\sigma_r}{G_s^*(\eta)} = \frac{(\Psi_0^2 - 2)}{R}\left[\frac{\partial u}{\partial \xi} + \frac{u}{\xi} + \frac{1}{\xi}\frac{\partial v}{\partial \theta}\right] + \frac{2}{R}\frac{\partial u}{\partial \xi} \quad (4a)$$

$$\frac{\sigma_\theta}{G_s^*(\eta)} = \frac{(\Psi_0^2 - 2)}{R}\left[\frac{\partial u}{\partial \xi} + \frac{u}{\xi} + \frac{1}{\xi}\frac{\partial v}{\partial \theta}\right] + \frac{2}{R}\left[\frac{u}{\xi} + \frac{1}{\xi}\frac{\partial v}{\partial \theta}\right] \quad (4b)$$

$$\frac{\tau_{r\theta}}{G_s^*(\eta)} = \frac{1}{R}\left(\frac{1}{\xi}\frac{\partial u}{\partial \theta} + \frac{\partial v}{\partial \xi} - \frac{v}{\xi}\right) \quad (4c)$$

$$\frac{\tau_{\theta z}}{G_s^*(\eta)} \approx \frac{1}{H}\frac{\partial v}{\partial \eta} \tag{4d}$$

$$\frac{\tau_{rz}}{G_s^*(\eta)} \approx \frac{1}{H}\frac{\partial u}{\partial \eta} \tag{4e}$$

in which $G_s^*(\eta) = G_s(\eta)\,(1 + 2i\beta_s)$ and Ψ_0 is a dimensionless parameter, solely function of the soil's Poisson's ratio ν_s (Veletsos & Younan 1994, Anoyatis et al. 2016)

$$\Psi_0 = \sqrt{\frac{2}{1-\nu_s}} \tag{5}$$

It is essential to note that the Tajimi solution to the problem assumes vanishing vertical displacements w (Tajimi 1969). The expressions for the various response quantities can now be derived from those presented herein by replacing the factor Ψ_0 with the appropriate factor Ψ_e, as shown below

$$\Psi_e = \sqrt{\frac{2(1-\nu_s)}{1-2\nu_s}} \tag{6}$$

This new factor represents the ratio of the dilatational and shear wave velocities in the soil medium. Notably, from Equations (4a) and (6), it can be observed that as ν_s approaches 0.5 (indicative of saturated soil conditions), the radial normal stresses σ_r, obtained in the solution for the $w = 0$ approximation, tend to infinity, an outcome that is inconsistent with physical reality.

Substituting the stresses (Eqs. 4) into the equations of motion (Eqs. 3) one gets:

$$\eta_L^2\,\frac{\partial}{\partial \xi}\left[\frac{1}{\xi}\left(\frac{\partial}{\partial \xi}(\xi u) + \frac{\partial v}{\partial \theta}\right)\right] - \frac{1}{\xi}\,\frac{\partial}{\partial \theta}\left[\frac{1}{\xi}\left(\frac{\partial}{\partial \xi}(\xi\, v) - \frac{\partial u}{\partial \theta}\right)\right] + \left(\frac{R}{H}\right)^2\left\{\frac{1}{G_s^*(n)}\,\frac{\partial}{\partial \eta}\left(G_s^*(n)\frac{\partial u}{\partial \eta}\right) + \left(\frac{\omega\, H}{V_s^*(\eta)}\right)^2 u\right\} = 0 \tag{7a}$$

and

$$\frac{\partial}{\partial \xi}\left[\frac{1}{\xi}\left(\frac{\partial}{\partial \xi}(\xi u_\theta) - \frac{\partial u_r}{\partial \theta}\right)\right] + \eta_L^2\,\frac{1}{\xi}\,\frac{\partial}{\partial \theta}\left[\frac{1}{\xi}\left(\frac{\partial}{\partial \xi}(\xi u_r) + \frac{\partial u_\theta}{\partial \theta}\right)\right] + \left(\frac{R}{H}\right)^2\left\{\frac{1}{G_s^*(n)}\,\frac{\partial}{\partial \eta}\left(G_s^*(n)\frac{\partial u_\theta}{\partial \eta}\right) + \left(\frac{\omega\, H}{V_s^*(\eta)}\right)^2 u_\theta\right\} = 0 \tag{7b}$$

where η_L is expressed as (Veletsos & Younan 1994)

$$\eta_L^2 = \frac{2 - \nu_s}{1 - \nu_s} \tag{8}$$

and $V_s^*(\eta) = V_s(\eta)\sqrt{(1 + 2i\beta_s)}$ is the complex-valued propagation velocity of shear waves in the soil medium.

For a harmonic excitation of circular frequency ω, the radial and tangential displacements can be expressed in the form

$$u(\xi, \theta, \eta, t) = U(\xi, \theta, \eta)\, e^{i\omega t} \tag{9a}$$

and

$$v(\xi, \theta, \eta, t) = V(\xi, \theta, \eta)\, e^{i\omega t} \tag{9b}$$

in which U and V represent the amplitudes of the resulting displacements relative to the moving rigid base. The functions $U(\xi, \theta, \eta)$ and $V(\xi, \theta, \eta)$ can be expressed as linear combinations of appropriately chosen eigenmodes of the soil-caisson system (Anoyatis et al. 2024a, Anoyatis et al. 2024b, Della Corte et al. 2024a, Della Corte et al. 2024b)

$$U(\xi, \theta, \eta) \;=\; \sum_{m=1}^{\infty} U_m(\xi) \cos\theta \;\; Y_m(\eta) \tag{10a}$$

and

$$V(\xi, \theta, \eta) \;=\; \sum_{m=1}^{\infty} V_m(\xi) \sin\theta \;\; Y_m(\eta) \tag{10b}$$

in which U_m and V_m are functions of only the radial position coordinate ξ, due to the symmetry of the system. The eigenmodes (eigenfunctions) Y_m satisfy the following differential equation (Tsikas 1995)

$$\frac{d}{d\eta}\left(G_s(\eta)\, \frac{dY_m}{d\eta}\right) + \; H^2\left(\frac{\omega^2\, \rho_s}{1 + 2i\beta_s} + \lambda_m\, G_s(\eta)\right) Y_m \;=\; 0 \tag{11}$$

and the boundary conditions of zero displacement at the rigid base and stress-free condition at the soil surface i.e., $Y_m(1) = 0$ and $dY_m/d\eta|_{\eta=0} = 0$. Equation (11) is a Sturm-Liouville (SL) equation with variable coefficients and its solution depends on the functional form of $G_s(\eta)$. Finding the distinct values λ_m $(m = 1, 2, 3, \ldots)$ for which non-trivial solutions to satisfy the boundary conditions exist, is part of the SL theory (Anoyatis et al. 2019). λ_m's are referred to as the eigenvalues of the boundary-value problem and specific solutions to Equation (11) are the eigenfunctions (soil modes) Y_m and can

be obtained in closed form in dynamic regime for specific types of soil inhomogeneity (Anoyatis et al. 2023).

Furthermore, one can deduce that the class of the eigenmodes $Y_m(\eta)$ is orthogonal with respect to the shear modulus $G_s^*(\eta)$, which is a weight function in SL-theory,

$$\int_0^1 G_s^*(\eta)\, Y_m(\eta)\, Y_k(\eta)\, d\eta = 0, \quad m \neq k \tag{12}$$

considering that the shear modulus must not vanish in the domain of the solution. Notice that the above expressions for *U* and *V* satisfy automatically the boundary conditions, $u|_{\eta=1} = v|_{\eta=1} = 0$.

Expressing U_m and V_m in terms of the potential functions Φ_m and Ψ_m

$$U_m = \frac{d\Phi_m}{d\xi} + \frac{\Psi_m}{\xi} \tag{13a}$$

and

$$V_m = -\frac{\Phi_m}{\xi} - \frac{d\Psi_m}{d\xi} \tag{13b}$$

and substituting Equations (13) into (10) and (9), and then into the governing equations (7), the solutions for U_m and V_m can be obtained, considering the conditions at the soil-caisson interface (Veletsos & Younan 1994).

At this stage, the concept of generalized soil impedance $\widetilde{K}_m$ can be introduced, which reflects the horizontal soil reaction at the soil-caisson interface (Tsikas 1995)

$$\widetilde{K}_m = -\int_0^{2\pi} [\sigma_m(1)\cos^2\theta - \tau_m(1)\ \sin^2\theta]\, R\, d\theta = -\pi R \left(\sigma_m(1) - \tau_m(1)\right) \tag{14}$$

where $\sigma_m(1) = \sigma_m(\xi = 1)$ and $\tau_m(1) = \tau_m(\xi = 1)$ are the stresses at the soil-caisson interface

$$\sigma_m(1) = \frac{G_s^*}{R}\{A_m[(\Psi_0^2\alpha_m^2 + 4)K_1(\alpha_m) + 2\alpha_m K_0(\alpha_m)] - 2B_m[2K_1(\beta_m) + \beta_m K_0(\beta_m)]\} \tag{15a}$$

and

$$\tau_m(1) = \frac{G_s^*}{R}\{-B_m[K_1(\beta_m)(\beta_m^2 + 4) + 2\beta_m K_0(\beta_m)] + 2A_m[2K_1(\alpha_m) + \alpha_m K_0(\alpha_m)]\} \tag{15b}$$

The constants A_m and B_m are determined by satisfying the boundary conditions $U_m|_{\xi=1} = 1$ and $V_m|_{\xi=1} = -1$:

$$A_m = -\frac{1}{\Delta_m}\,[2K_1(\beta_m) + \beta_m K_0(\beta_m)] \tag{16a}$$

and

$$B_m = -\frac{1}{\Delta_m}\,[2K_1(\alpha_m) + \alpha_m K_0(\alpha_m)] \tag{16b}$$

where the parameter Δ_m is obtained from the following expression

$$\Delta_m = [K_1(\alpha_m) + \alpha_m K_0(\alpha_m)]\;\;[K_1(\beta_m) + \beta_m K_0(\beta_m)] \;-\; K_1(\alpha_m)\;K_1(\beta_m) \tag{16c}$$

In the above equations $K_v(\,)$ denotes the modified Bessel function of the second kind and order v (Abramowitz & Stegun), and $\alpha_m = (R/\Psi_0)\sqrt{\lambda_m}$ and $\beta_m = \Psi_0\,\alpha_m$, where a_m and λ_m are obtained from the solution of the partial differential equations of motion (Eqs. 7) using the methods of Helmholtz decomposition and separation of variables.

The impedance $\widetilde{K}_m$ represents the amplitude of harmonic circumferential force necessary to induce a steady-state circumferential displacement of unit amplitude. It depends on the characteristics of the system and the frequency of excitation. The real part of $\widetilde{K}_m$ represents the force component that is in phase with the excitation, whereas the imaginary part represents the component that is 90° out of phase. In the conventional spring-dashpot representation of the resisting action of the medium, the stiffness of the spring is represented by $Re(\widetilde{K}_m)$ and the coefficient of the viscous damper C by $Im(\widetilde{K}_m)/\omega$.

The proposed solution accounts for the boundary conditions of zero tractions at the soil surface and bounded displacements at large radial distances from the caisson. It should be noted that Equation (2c), which expresses the equilibrium of the vertical ("parasitic") forces, is not satisfied in this approach, nor is the condition of vanishing shears $\tau_{r\theta}$ at the soil surface. The literature contains numerous examples of similar violations associated with "parasitic" stresses, which exert only a minor influence on the solution (e.g., Veletsos & Younan 1994, Tajimi 1969, Nogami & Novak 1977, Anoyatis et al. 2016).

At this point the steady-state response of the caisson to a harmonic base motion, along with the corresponding response of the soil stratum, can be readily evaluated. Utilizing the same assumptions as previously, the radial and tangential displacements at the far-field may be expressed as follows

$$u_{\xi\to+\infty} = U_{ff}(\eta)\cos\theta\;\; e^{i\omega t} \tag{17a}$$

and

$$v_{\xi \to +\infty} = -U_{ff}(\eta) \sin\theta \; e^{i\omega t} \tag{17b}$$

in which

$$U_{ff}(\eta) \; = \; - \frac{\rho_s \left(\ddot{u}_g\right)_m}{\lambda_m} \, Y_m(\eta) \; = \; \left(U_{ff}\right)_m \, Y_m(\eta) \tag{18}$$

is the displacement amplitude of a vertical cantilever shear beam of the same height and material properties as the soil stratum at hand, excited at its base. The term $(\ddot{u}_g)_m$ is determined by decomposing the acceleration $\ddot{u}_g(t)$ using the following transformation, based on generalized Fourier series expansion (Courant & Hilbert 1953, Anoyatis et al. 2024b)

$$\ddot{u}_g(t) = \; (\ddot{u}_g)_m \; G_s^*(\eta) \; Y_m(\eta) \; e^{i\omega t} \tag{19}$$

where

$$(\ddot{u}_g)_m \; = \; \frac{\ddot{u}_g \; \int_0^1 Y_m \, d\eta}{\int_0^1 G_s^* \; Y_m^2 \; d\eta} \tag{20}$$

The force per unit height of the caisson, parallel to the direction of motion, can be obtained by multiplying each displacement component by the corresponding impedance. Accordingly, it is deduced that

$$P(\eta, t) = \sum_{m=1}^{+\infty} \widetilde{K}_m \left(U_{ff}\right)_m \, Y_m \, e^{i\omega t} \tag{21}$$

in which a positive $P(\eta, t)$ is considered to coincide with the direction of the base motion. Finally, the expressions for the shear force $Q(\eta, t)$ and the bending moment $M(\eta, t)$ across a normal section are determined from the following expressions

$$Q(\eta, t) \; = \int_0^{\eta} P(\eta_0, t) \; H \; d\eta_0 \; = \; \int_0^{\eta} \widetilde{K}_m \left(U_{ff}\right)_m \, Y_m|_{\eta=\eta_0} \, e^{i\omega t} \; H \; d\eta_0 \tag{22}$$

and

$$M(\eta, t) \; = \int_0^{\eta} P(\eta_0, t) \; \eta_0 \; H^2 \; d\eta_0 \; = \; \int_0^{\eta} \widetilde{K}_m \left(U_{ff}\right)_m \, Y_m|_{\eta=\eta_0} \, e^{i\omega t} \; \eta_0 \; H^2 \; d\eta_0 \tag{23}$$

With the harmonic response of the system established, the response to an arbitrary transient excitation is computed using the Discrete Fourier Transform (DFT) method in combination with the Fast Fourier Transform (FFT) algorithm. To implement this procedure, the duration of the forcing function is extended by appending a sufficiently long band of zeros to prevent aliasing errors that could otherwise occur (Chopra 1995, Cooley & Tukey 1965, Veletsos & Ventura 1985).

NUMERICAL RESULTS

STATIC EFFECTS

To illustrate the effects of soil inhomogeneity on the system response, four soil profiles with the same average shear modulus G_0 are considered (Fig. 2). This form of inhomogeneity captures, in a simple manner, not only the reduction in soil stiffness due to the lower confining pressures near the soil surface, but also the softening of the soil resulting from large shear deformations and the nonlinear behavior at the soil-caisson interface, including separation and slippage. All the results are obtained using a Poisson's ratio $\nu_s = 1/3$ for the soil, unless otherwise stated.

The analysis starts by investigating the system's response to harmonic excitations with frequencies much lower than the fundamental natural frequency of the soil stratum (i.e., $\omega \to 0$), referred to as "pseudo-static" response. These results can be directly compared to available pseudo-static soil mechanics solutions.

Figure 3 presents the first three "static" mode shapes Y_m $(m = 1, 2, 3)$ for the four types of soil inhomogeneity shown in Figure 2. The modes are obtained from the solution to Equation (11) and are normalized to their value at the soil surface. It is evident that the mode shapes vary significantly with increasing inhomogeneity. For a homogeneous profile (soil 1), the fundamental mode Y_1 attains its maximum at the soil surface, while for increasingly inhomogeneous profiles, the maximum shifts deeper, occurring around mid-depth in strongly inhomogeneous cases.

Figure 4 presents the maximum values of the static resultant force per unit of height $(P_x)_{stat}$, as a function of the soil stratum height H to caisson radius R. The results indicate that the magnitude of the resultant force increases monotonically with increasing H/R. Additionally, for a homogeneous soil with a shear modulus equal to the average G_0 of the inhomogeneous profiles analyzed, the resultant forces for the homogeneous soil are consistently higher than those for the inhomogeneous profiles across the entire range of H/R ratios investigated. This suggests soil inhomogeneity leads to reduced caisson pressures compared to the homogeneous case. This reduction seems largely independent of the specific type of inhomogeneity or variation in shear modulus, provided that G_0 remains constant.

Figure 5 presents the variation with normalized depth z/H of the normalized pseudo-static force per unit height $(P_x)_{stat}$ for the selected soil profiles and H/R ratios (i.e., $H/R = 0,\ 1,\ 3$). For the

homogeneous profile (soil 1), $(P_x)_{stat}$ decreases monotonically with depth. In contrast, for all other types of soil inhomogeneity investigated, $(P_x)_{stat}$ reaches a maximum at a certain depth below the surface. The exact location and magnitude of this maximum depend on the type of inhomogeneity and the soil-caisson system geometry. Higher H/R values consistently correspond to higher maxima, while stronger inhomogeneity shifts the position of the maximum to greater depths.

In cases where the system's response is approximated by considering the contribution of only the fundamental mode, the interface forces would have been proportional to $G_s^*(\eta)\, Y_1(\eta)$, with the distribution of shearing forces and bending moments determined by the following expressions

$$Q_b(\eta) \;=\; Q_b\, G_s(\eta)\, \frac{\partial Y_1}{\partial \eta}(\eta) \tag{24}$$

and

$$M_b(\eta) \;=\; M_b \int_0^{\eta} \int_0^{\eta_1} G_s(\eta_2)\, Y_1(\eta_2)\, d\eta_2 \tag{25}$$

The corresponding approximate results for Q_b and M_b (as defined in Eqs. (24) and (25), respectively) are presented in Figures 6 and 7. These figures illustrate the results for various soil profiles, characterized by differing degrees of inhomogeneity (Fig. 2) and geometries defined by the H/R ratio.

Figure 6 illustrates the variations of the normalized pseudo-static shear force with the depth along the caisson embedded in different soil types (as shown in Fig 2) for selected height-to-radius ratios H/R of 1 and 3. The shear force distribution is plotted against the normalized depth z/H. A common trend is observed for all cases: the shear force increases with increasing depth, attaining its maximum at the caisson base. There is a noticeable stronger increase in the shear forces with depth for the slenderer caisson ($H/R = 3$). It is evident that the highest forces develop for a caisson embedded in a homogeneous soil layer (Soil 1), of constant soil shear modulus equal to the average moduli of the inhomogeneous layers investigated. It is evident that Q_{st} values drop with increasing soil inhomogeneity.

Likewise, Figure 7 presents the variations of the normalized pseudo-static bending moment with depth along the caisson embedded in the same soil types and for the same height-to-radius ratios as in Figure 6. Similarly to the shear forces, the bending moments increase with increasing depth, reaching their maximum at the caisson base. A pronounced increase in bending moments with depth is observed for the more slender caisson ($H/R = 3$), for all types of inhomogeneity investigated. The highest bending moments clearly developed for homogeneous soil (Soil 1). Additionally, there is a clear reduction in M_{st} values with increasing degrees of soil inhomogeneity.

HARMONIC RESPONSE

Figure 8(a) shows the variation with the dimensionless frequency $a_0 = \omega R/\bar{V}_s$ of the force amplitude (per unit height), normalized by its static value (i.e., $a_0 = 0$) and induced at the middle ($z/H = 1/2$) of the caisson, for a harmonically excited soil-caisson system, where $\bar{V}_s$ stands for the propagation velocity of a reference shear wave in the soil medium with average soil shear modulus G_0 (i.e., $\bar{V}_s = \sqrt{G_0/\rho_s}$). Results are shown for three different soil-caisson geometries namely $H/R = 0.5, 1, 2, 3$ and soil 4 type inhomogeneity (Fig. 2) soil with material damping of $\beta_s = 5\%$.

The following main trends are observed: In the low frequency range ($\omega < \omega_1$, ω_1 being the first natural frequency for the soil layer), the force amplitude is dominated by its real part, whereas for frequencies higher than the resonance ($\omega \geq \omega_1$), the contribution of the imaginary part becomes more important. In particular, the rapid and significant increase of the imaginary part in the vicinity of ω_1 is well-documented in the literature (Gazetas & Tassoulas 1987, Guan & Novak 1994, Assimaki et al. 2001). This is attributed to the fact that no energy dissipates by radiation (emergence of travelling waves) within this frequency range. As expected, the absolute maximum values of the force amplitude are attained at resonance ($\omega = \omega_1$). The amplification values range between 3.5 and 5 for all soil profiles investigated. Note that an amplification factor attains its minimum value of approximately 3.13 in the limiting case of $H/R \to 0$, which corresponds to the scenario of a rigid retaining wall ($H/R \to \infty$) rather than a caisson. This value of amplification is consistent with that reported in Veletsos & Younan (1994a) for the corresponding dynamic soil-wall interaction problem. The relative low values observed indicate greater damping in the plane strain soil-wall system compared to the (approximate) three-dimensional anti-symmetric soil-caisson system. This finding aligns with the differences in radiation damping between a strip foundation in plane-strain conditions, and a circular foundation subjected to horizontal loading in anti-symmetric mode, as documented by Gazetas (1982) and (1987).

Having examined the trends in lateral forces along the caisson with varying excitation frequencies and transitions between the natural frequencies of the system, it is now pertinent to delve into the mathematical aspects. The analysis can provide insight into how inhomogeneity influences the resonances, by using the proposed model to determine the free-field response and, thus, its resonances. In this regard, values for the m-th dimensionless natural frequencies $a_{0,m}$ are presented in Table 1, for the inhomogeneity patterns shown in Figure 2. An increase in the fundamental frequency ω_1 is observed as the degree of inhomogeneity increases, whereas the trend reverses for higher natural frequencies (e.g., ω_2 and ω_3). It is noteworthy that the amplification is slightly higher in homogeneous soil, which contrasts with the trend observed in the free-field soil amplification of motion as reported by Gazetas (1982) and (1987), in which stronger inhomogeneity results in larger amplification.

The effect of the slenderness ratio (H/R) on the amplification factor at resonance is shown in Figure 8(b). The results are presented for H/R values ranging from 1 to 3. It is noteworthy that increasing H/R slightly increases the amplification factor at resonance for all soil inhomogeneity profiles. This observation, initially noted by Veletsos & Younan (1994b), parallels the effect of decreasing damping on the transmissibility factor of a viscously damped single-degree-of-freedom system. Specifically, for fixed soil stratum thickness, reducing the caisson's radius reduces the lateral surface area of the caisson, thereby decreasing system's capacity to radiate energy (radiation damping).

The variations in force amplitude along depth for the soil-caisson systems considered in Figure 8, are shown in Figure 9, for different values of the dimensionless frequency ratio a_0. The results are normalized with respect to the maximum absolute static value of the force. It is observed that for frequency ratio values within the range $0 \leq \mathrm{a}_0 \leq 1$, the force attains smaller values at zero frequency along the caisson and increases gradually, matching the shape of the first mode of vibration $Y_1(\eta)$. The force distribution follows a wave-like pattern, starting from zero at the base to a finite value at the surface similar to $Y_1(\eta)$. This indicates that the fundamental mode of vibration of the soil-caisson is dominating and hence controls the system's response. For larger a_0 values, the distribution is wavy due to the increased participation of higher modes of vibration. However, even in these cases, the contribution of the fundamental mode remains substantial.

Figure 10 presents the variation of the caisson base shear normalized both over its static value (amplification factor $Q_b/Q_{b,st}$), and the base excitation ($Q_b/\pi\rho_s\ddot{u}_g RH^2$), as function of the dimensionless frequency ratio a_0, for a soil-caisson system of $H/R = 3$. Evidently, as shown in the subfigures, the impact of inhomogeneity on peak amplification does not exceed 40 %, with the homogeneous case exhibiting the highest amplification.

Figure 11 presents the variation with the dimensionless frequency ratio a_0 of the height h of application of the resultant horizontal force acting on the caisson, normalised by the caisson height H, for caisson slenderness ratio $H/R = 3$ and different soil profiles. Four distinct curves are plotted, each representing a different soil inhomogeneity type labelled as Soil (1), Soil (2), Soil (3), and Soil (4) (Fig. 2). Overall, it is evident that there is a strong effect of excitation frequency on h, while the effect of inhomogeneity is less pronounced. At $\mathrm{a}_0 = 0$, all soil types start with h/H values around approximately $0.5 - 0.6$, indicating similar behavior for "static" conditions. As a_0 increases from 0 to 1, there is a slight increase in h/H values, accompanied by a noticeable drop for all soil types, with Soil (1) showing the most pronounced decrease at the first resonant frequency of the system ($\mathrm{a}_0 \approx 1.5$). Beyond the first resonance, the curves exhibit a recovery, with h/H values increasing again, though return to values lower than their initial (static) levels. In the vicinity of $\mathrm{a}_0 = 2.5$, another dip is observed, which is associated with the second resonance of the system. Particularly for Soil (1), a distinct drop compared to the other soils is observed. For higher excitation frequencies ($\mathrm{a}_0 \gtrsim 3$), the curves tend to

stabilize, with minor fluctuations, indicating the gradually suppressed role of higher resonances in the point of application of the resultant horizontal force.

TRANSIENT RESPONSE

The response of the soil-caisson system is also evaluated using the ground motion recorded during the 6.4-magnitude earthquake recorded on August 14, 2003 in Lefkada, Greece. The peak ground acceleration was $\ddot{u}_g = 0.425\ g$ (Fig. 12(a)) and the maximum spectral acceleration, obtained from the response spectrum using the commonly used 5 % damping for most structures, was found to be $1.6\ g$ at a period of $T \approx 0.36\ s$ (Fig. 12(b)). Figure 12(c) depicts the amplification factor for the maximum amplitude of the base shear ($Q_b/Q_{b,st}$) acting on a caisson with $H/R = 3$ and subjected to this earthquake motion at its base. The static values of the base shear can be computed by interpreting $\ddot{u}_g$ as the maximum acceleration of the transient ground motion. The results are plotted as a function of the fundamental frequency of the soil stratum f_1. For very stiff strata with $f_1 \approx 5\ Hz$, the amplification factors are approximately equal to one. As the system frequency decreases, the amplification factors generally increase for all soil profiles. This behavior is consistent with observations made for harmonically exited soil-caisson systems. For highly compliant systems with very low natural frequencies, the amplification factors drop naturally below one.

CONCLUSIONS

A rigorous analytical solution has been developed for the dynamic response of an end-bearing rigid caisson in an inhomogeneous soil stratum resting on a rigid base. The proposed extends the seminal work of Veletsos & Younan (1994b) to derive a novel semi-analytical solution to account for soil inhomogeneity. The results converge to the solution of Veletsos & Younan (1994a, 1998) for caissons in homogeneous soils. The approach neglects the equilibrium of the soil in the direction perpendicular to the loading yet allows the solution to be obtained in a semi-closed form. Despite these restrictions, the model is physically sound and can capture the key aspects governing the seismic response of rigid caissons. The model can serve as a benchmark solution to allow verifications of more complex dynamic numerical models and provides additional valuable insights into the dynamic response of caissons embedded in non-homogeneous soils layers. With the novel semi-analytical expressions developed herein, the dynamic pressures and associated base shears and bending moments induced by ground shaking on caissons can be easily evaluated. The resultant soil reaction force per unit height is shown to be a function of the caisson's slenderness ratio H/R, type of soil inhomogeneity, and, evidently, excitation frequency. The model, with minor modifications, has further taken into account actual recorded motions at the bedrock and generated a response spectrum for the amplification of the base shear, while it can generate time histories of normal stresses, total forces, and moments that develop on

caissons. Finally, it is essential to point out that limiting case of $H / R \to 0$, corresponds to the scenario of a rigid retaining wall ($H / R \to \infty$), rather than a caisson, and the results are consistent with that reported in Veletsos & Younan (1994a) for the corresponding dynamic soil-wall interaction problem.

REFERENCES

Abramowitz M & Stegun IA. Handbook of mathematical functions, Dover Publications, New York, (1972).

Anoyatis G, Mylonakis G & Lemnitzer A (2016). Soil reaction to lateral harmonic pile motion. *Soil Dynamics and Earthquake Engineering*, 87:164-179. https://doi.org/10.1016/j.soildyn.2016.05.004

Anoyatis G, Mylonakis G & Tsikas A (2019). An analytical continuum model for axially loaded end-bearing piles in inhomogeneous soil. *International Journal for Numerical and Analytical Methods in Geomechanics*, 43(6):1162-1183. https://doi.org/10.1002/nag.2886

Anoyatis G, François S, Orakci O & Tsikas A (2023). Soil-pile interaction in vertical vibration in inhomogeneous soils. *Earthquake Engineering & Structural Dynamics*, 52(14):4582-4601. https://doi.org/10.1002/eqe.3968

Anoyatis G, Della Corte A, Orakci O, Di Laora R, Tsikas A, François S (2024a). Kinematic response of end-bearing piles in inhomogeneous soils under P-wave excitation. *Japanese Geotechnical Society Special Publication*, 2024, 10(55):2078-2083.Publication date 2024/06/17, Online ISSN 2188-8027, https://doi.org/10.3208/jgssp.v10.OS-44-05.

Anoyatis G, François S, Letizia N, Della Corte A, Orakci O, Tsikas A (2024b). Seismic soil pressures on rigid walls retaining inhomogeneous backfills. *18th World Conference on Earthquake Engineering (WCEE2024)*. Technical Session: GEO - geotechnical earthquake engineering and site response. Milan, Italy, 30 June to 5th July 2024.

Asimaki D, Chatzigiannelis Y, Gerolymos N & Gazetas G (2001). Lateral response of caisson foundations". Proceedings of the 4th Hellenic Conference on Geotechnical and Geoenvironmental Engineering, Athens, 2:115-122.

Varun, Assimaki D & Gazetas G (2009). A simplified model for lateral response of large diameter caisson foundations—Linear elastic formulation. Soil Dynamics and Earthquake Engineering, 29(2):268-291. ISSN 0267-7261, https://doi.org/10.1016/j.soildyn.2008.02.001.

Apsel R & Luco J (1987). Impedance functions for foundations embedded in a layered medium: an integral equation approach. *Earthquake Engineering & Structural Dynamics*, Vol. 15, pp. 213-231. https://doi.org/10.1002/eqe.4290150205.

Beredugo Y& Novak M (1972). Coupled horizontal and rocking vibration of embedded footings. *Canadian Geotechnical Journal*, 9:447-497. https://doi.org/10.1139/t72-046.

Chopra A, Dynamics of structures: Theory and applications to earthquake engineering, Prentice-Hall 1995.

Cooley J W & Tukey J W (1965). An algorithm for the machine calculation of complex Fourier series. *Mathematics of computation*, 19(1):297-301. https://doi.org/10.2307/2003354.

Courant R & Hilbert D. Methods of Mathematical Physics, Volume I, Interscience Publishers (division of John Wiley & Sons), INC, New York, (1953).

Day S & Frazier G (1979). Seismic response of hemispherical foundation. *Journal of the Engineering Mechanics Division*, ASCE, 105(1):29-41. https://doi.org/10.1061/JMCEA3.0002456.

Della Corte A, Orakci O, Tsikas A, François S, Anoyatis G (2024a). A semi-analytical model for axial soil-pile interaction in generalized inhomogeneous soils. *Proceedings of the XVIII ECSMGE 2024 Geotechnical engineering challenges to meet current and emerging needs of society*. ISBN 978-1-032-54816-6, DOI 10.1201/9781003431749-58. p. 438-443. 26-30 August, Lisbon, Portugal.

Della Corte A, Letizia N, Tsikas A, François S, Anoyatis G. (2024b). Dynamic soil pressures on rigid vertical walls in presence of generalized inhomogeneous soils. Under revision.

Dominguez J (1978). Response of embedded foundations to traveling waves. Report R78-24, Department of Civil Engineering, Massachusetts Institute of Technology.

Gazetas G (1982). Vibrational characteristics of soil deposits with variable wave velocity. *International Journal for Numerical and Analytical Methods in Geomechanics*, 6(1):1-20. https://doi.org/10.1002/nag.1610060103.

Gazetas G (1987). Simple physical methods for foundation impedances, Dynamic behaviour of foundations and buried structures, *Elsevier Applied Science*, Chapter II, pp. 45-93, P. K. Banerjee & R. Butterfield, editors.

Gazetas G & Tassoulas J (1987). Horizontal stiffness of arbitrarily shaped embedded foundations. *Journal Geotechnical Engineering, ASCE*, 113(5):440-457. https://doi.org/10.1061/(ASCE)0733-9410(1987)113:5(440).

Gerolymos N & Gazetas G. (2006a). Winkler model for lateral response of rigid caisson foundations in linear soil. *Soil Dynamics and Earthquake Engineering*, 26(5):347-361. ISSN 0267-7261, https://doi.org/10.1016/j.soildyn.2005.12.003.

Gerolymos N & Gazetas G (2006b). Development of Winkler model for static and dynamic response of caisson foundations with soil and interface nonlinearities. *Soil Dynamics and Earthquake Engineering*, 26(5):363-376. ISSN 0267-7261, https://doi.org/10.1016/j.soildyn.2005.12.002.

Gerolymos N & Gazetas G (2006c). Static and dynamic response of massive caisson foundations with soil and interface nonlinearities-validation and results. *Soil Dynamics and Earthquake Engineering*, 26(5):377-394. ISSN 0267-7261, https://doi.org/10.1016/j.soildyn.2005.12.001.

Guan F & Novak M (1994). Transient response of a group of rigid strip surface foundations. *Earthquake Engineering and Structural Dynamics*, 23(6):671-685. https://doi.org/10.1002/eqe.4290230607.

Harada T, Kubo K & Katayama T (1981). Dynamic soil-structure interaction analysis by continuum formulation method. Report of the Institute Science, the University of Tokyo, Vol. 29, No. 5.

Harada T, Kubo K & Katayama T (1985). Model of the effective seismic motions of embedded foundation and its verification by observed data. Proceedings, Japanese Society of Civil Engineers, 362:435-440.

Latini C & Zania V (2017). Dynamic lateral response of suction caissons. *Soil Dynamics and Earthquake Engineering*, 100, 59-71, ISSN 0267-7261, https://doi.org/10.1016/j.soildyn.2017.05.020.

Luco J & Wong H. Seismic response of foundations embedded in a layered half-space. *Earthquake Engineering & Structural Dynamics*, 15(2):233-247. https://doi.org/10.1002/eqe.4290150206.

Menahem A B & Singh S J. Seismic waves and sources, Springer Verlag, New York, 1981.

Nogami T & Novak M (1977). Resistance of soil to a horizontally vibrating pile. *Earthquake Engineering & Structural Dynamics*, 5(3):249-261. https://doi.org/10.1002/eqe.4290050304.

Pais A & Kausel E (1988). Approximate formulas for dynamic stiffness of rigid foundations. *Soil Dynamics & Earthquake Engineering*, 7(4):213-227. https://doi.org/10.1016/S0267-7261(88)80005-8.

Saitoh M. Effective seismic motion of caisson and pile foundation, Railway Technical Research Institute (RTRI), Report No. 46, Japan (2001).

Tajimi H. Dynamic analysis of a structure embedded in an elastic stratum", Proceedings of 4th World Conference Earthquake Engineering, Santiago, Chile, Vol. III (A-6), pp. 53-69, 1969.

Tassoulas J & Kausel E (1983). On the effect of the rigid sidewall on the dynamic stiffness of embedded circular footings. *Earthquake Engineering & Structural Dynamics*, 11(3):403-414. https://doi.org/10.1002/eqe.4290110307.

Timoshenko S P & Goodier J N. Theory of elasticity, McGraw-Hill, Inc., 1987.

Tsikas A (1995). Dynamic Modeling and Response of Rigid Embedded Cylinders in Inhomogeneous Soil (Master's thesis, in Greek). National Technical University of Athens (NTUA).

Veletsos S A & Ventura E C (1985). Dynamic analysis of structures by the DFT method. *Journal of Structural Engineering*, ASCE, 11(12):2625-2642. https://doi.org/10.1061/(ASCE)0733-9445(1985)111:12(2625).

Veletsos A & Younan A (1994a). Dynamic soil pressures on rigid vertical wall. *Earthquake Engineering & Structural Dynamics*, 23(3):275-301. https://doi.org/10.1002/eqe.4290230305.

Veletsos A & Younan A (1994b). Dynamic soil pressures on rigid cylindrical vaults. *Earthquake Engineering and Structural Dynamics*, 23(6):645-669. https://doi.org/10.1002/eqe.4290230606.

Wolf J P & Somaini D R (1986). Approximate dynamic model of embedded foundation in time domain. *Earthquake Engineering & Structural Dynamics*, 14(5), 683-703. https://doi.org/10.1002/eqe.4290140502

Younan A & Veletsos A (1998). Dynamic of solid-containing tanks. I: rigid tanks. *Journal of Structural Engineering*, 124(1):52-61. https://doi.org/10.1061/(ASCE)0733-9445(1998)124:1(52).

FIGURES

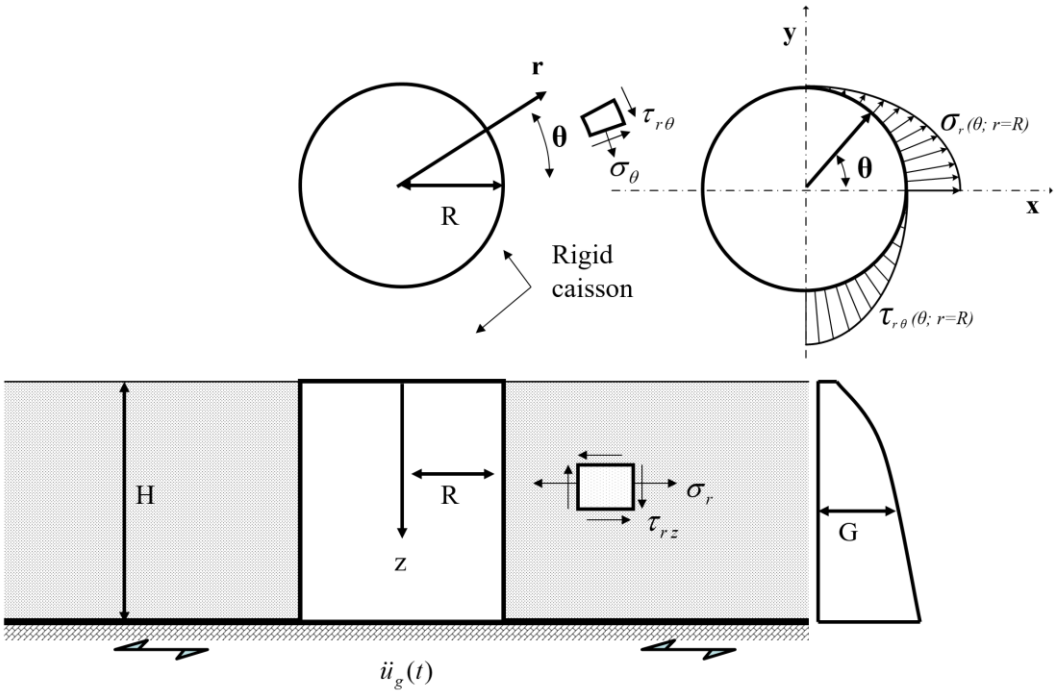

Figure 1. System considered; schematic distribution of the radial (σ_r) and the tangential ($\tau_{r\theta}$) components of the soil stresses as a function of θ, along a quarter of the caisson's circumference.

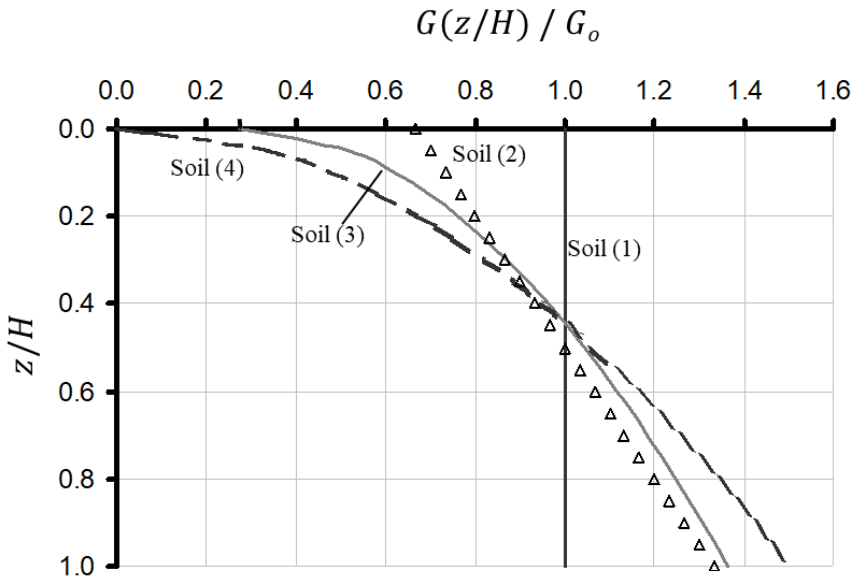

Figure 2. Four soil profiles considered in this study, characterized by a common average shear modulus G_0.

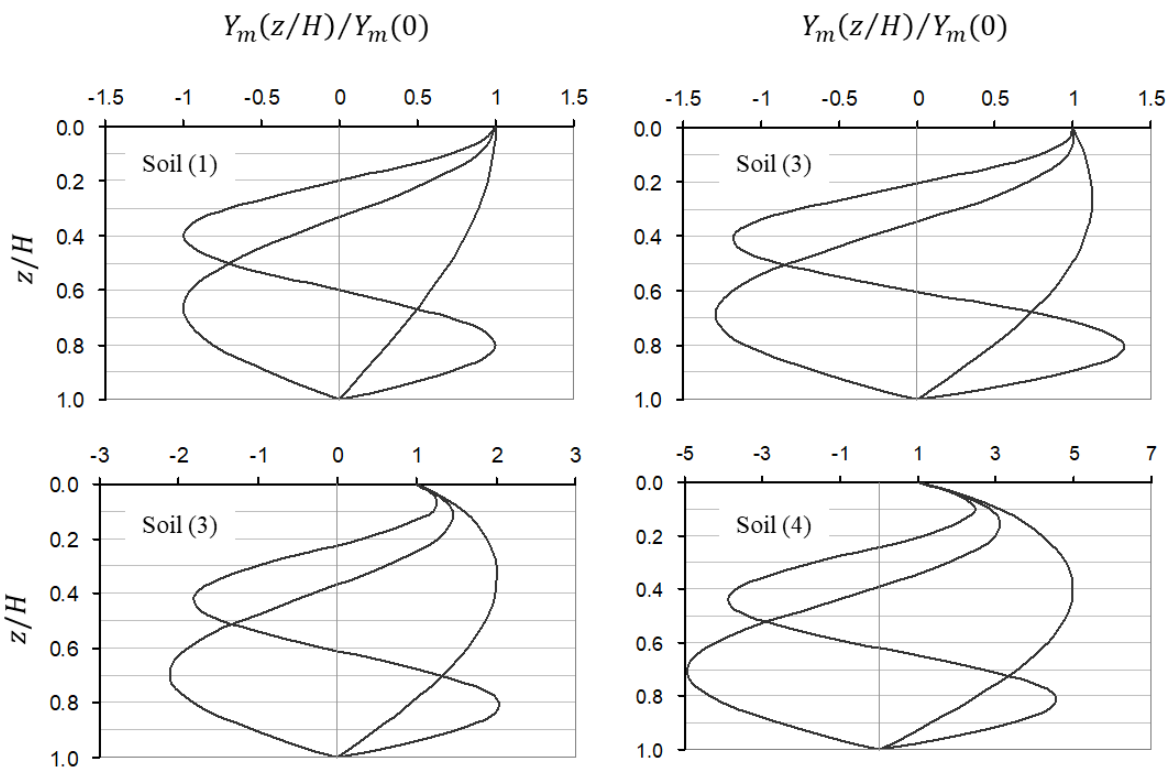

Figure 3. Variation of the first three "static" eigenmodes with depth for a homogeneous soil and selected types of soil inhomogeneity.

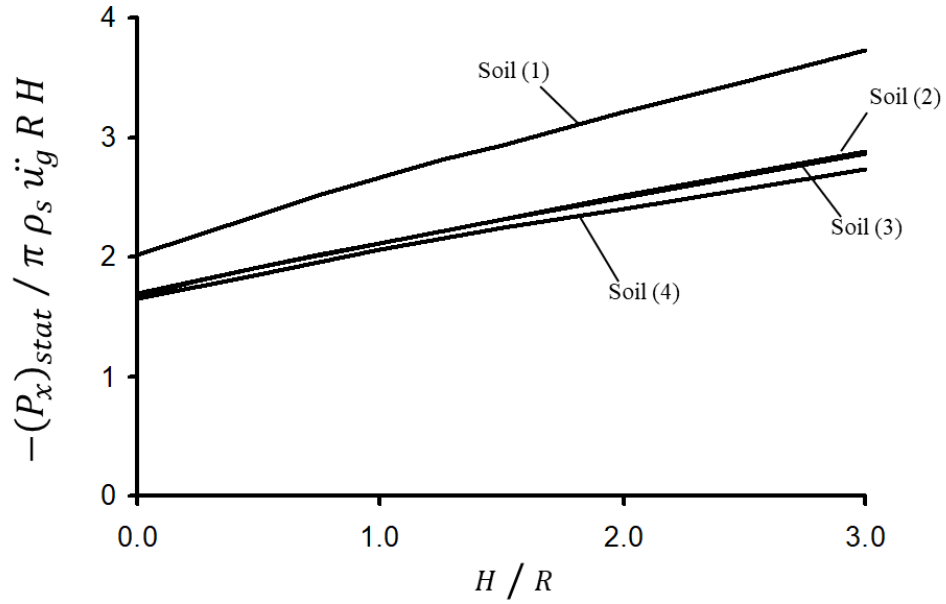

Figure 4. Variation with H/R ratio of the maximum values of the static resultant horizontal force per unit height, parallel to the direction of the motion induced on the caisson, for selected types of soil inhomogeneity.

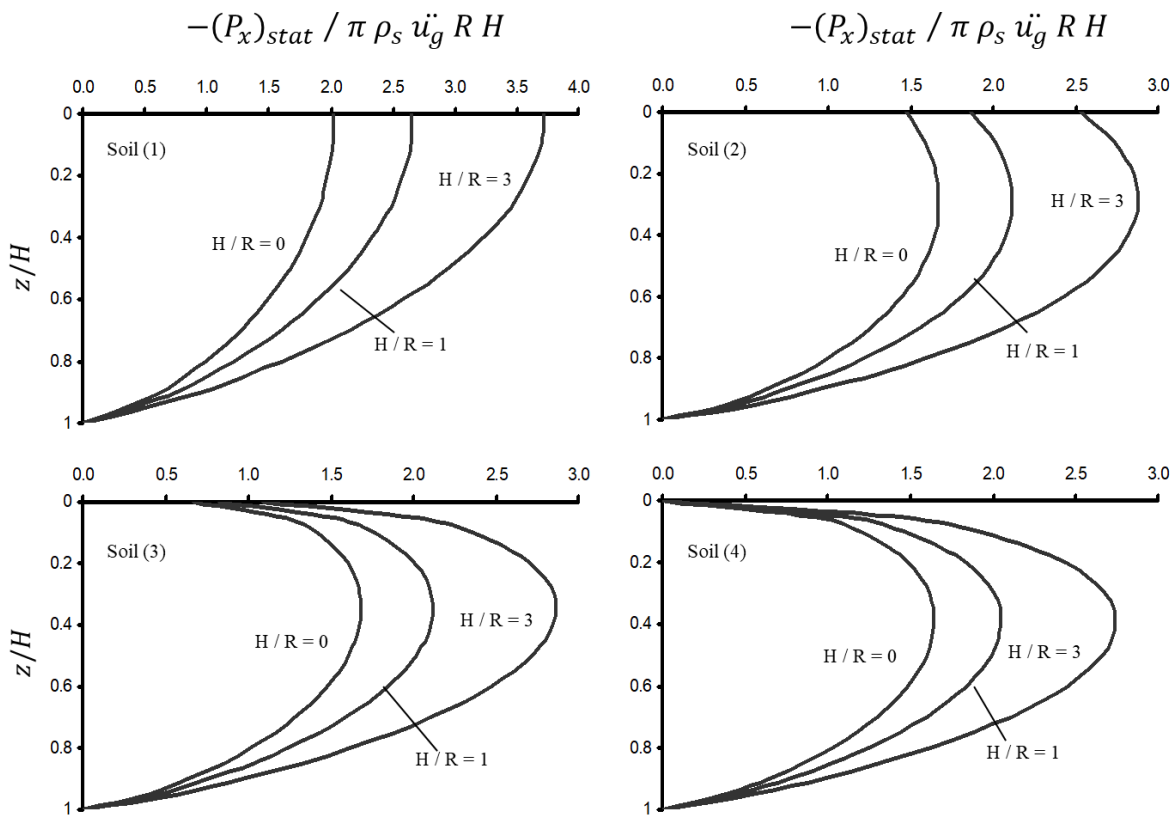

Figure 5. Variation with depth z/H of the normalized pseudo-static force per unit height $(P_x)_{stat}$ for the selected soil profiles and H/R ratios.

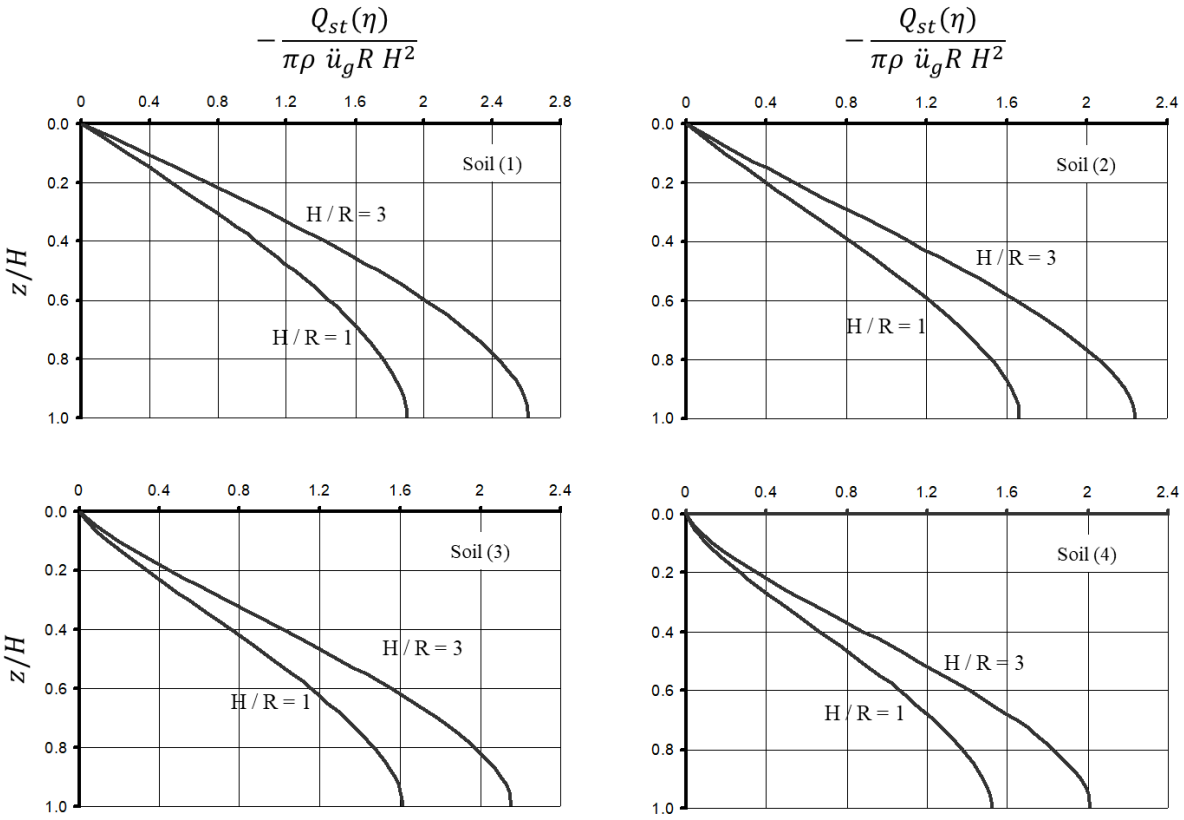

Figure 6. Variations of the pseudo-static shear force with depth along the caisson.

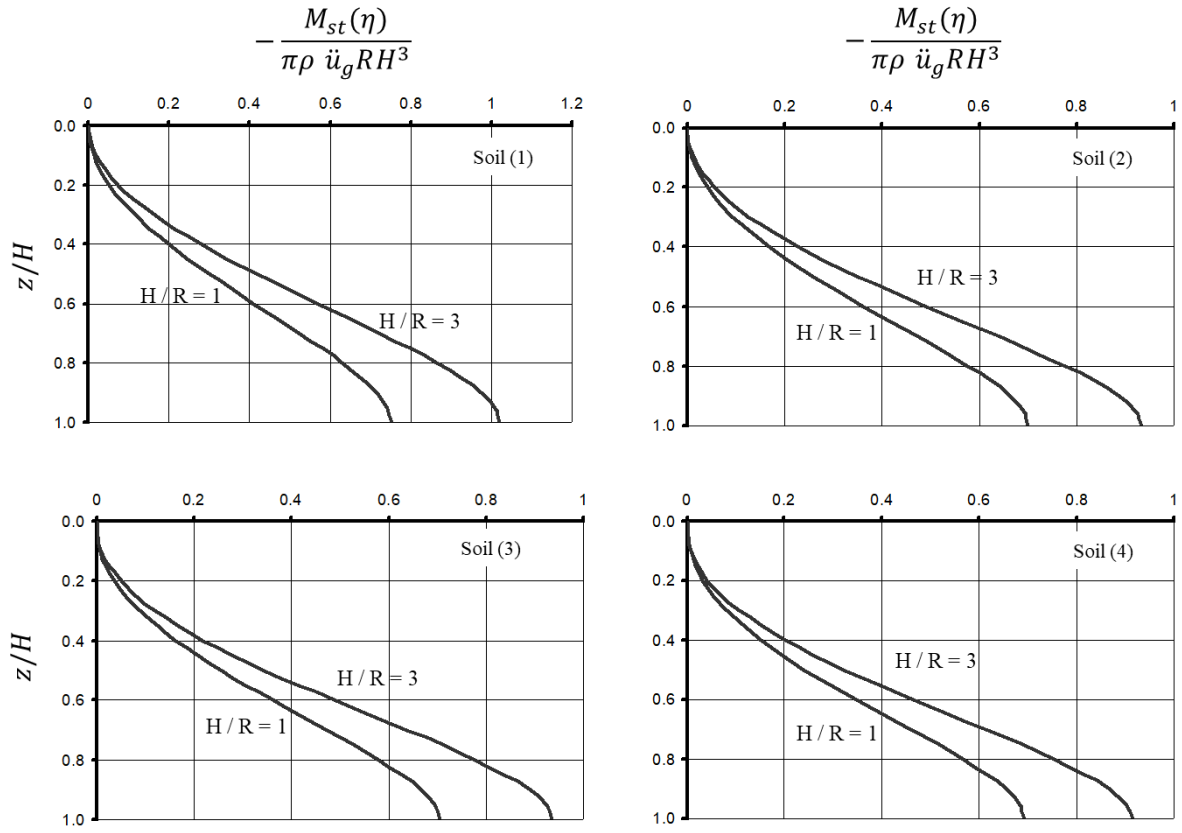

Figure 7. Variations of the pseudo-static bending moment with depth along the caisson.

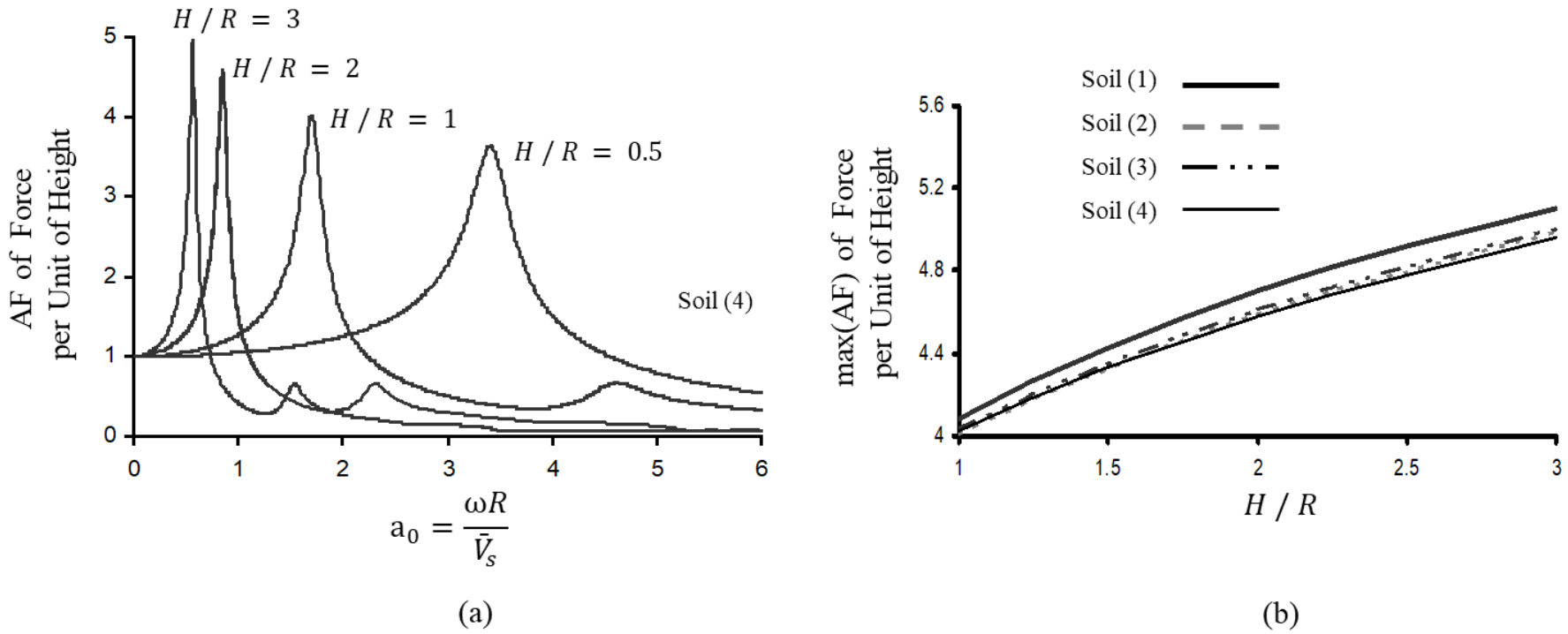

Figure 8. (a) Amplification factor of force per unit of height induced mid-depth ($z/H = 1/2$) of a harmonically excited rigid caisson for $H/R = 0.5, 1, 2, 3$ and $\beta_s = 5$ %. (b) Effect of slenderness ratio H/R on the amplification factor at resonance ($\omega = \omega_1$).

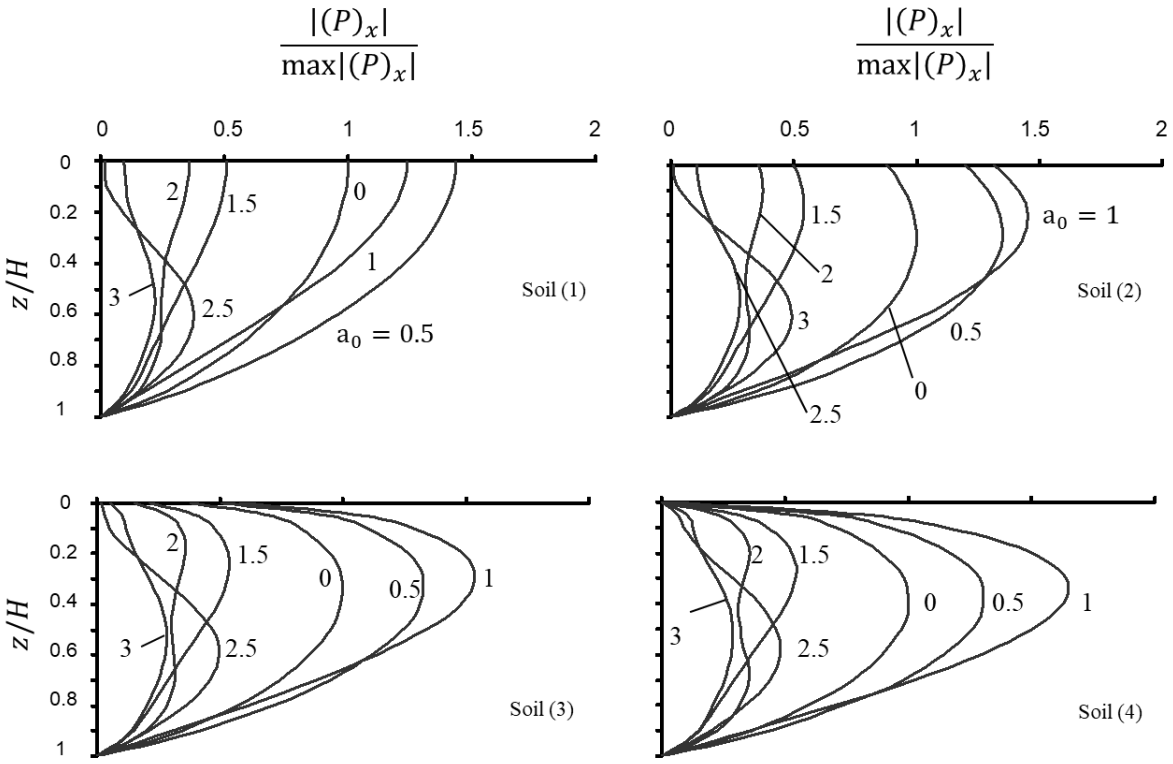

Figure 9. Variations along the depth of real valued amplitude of force per unit height induced on harmonically excited caisson for $H/R = 2$ and $\beta_s = 5$ %, and selected excitation frequencies $a_0 = 0,\ 0.5,\ 1,\ 1.5,\ 2,\ 2.5,\ 3$.

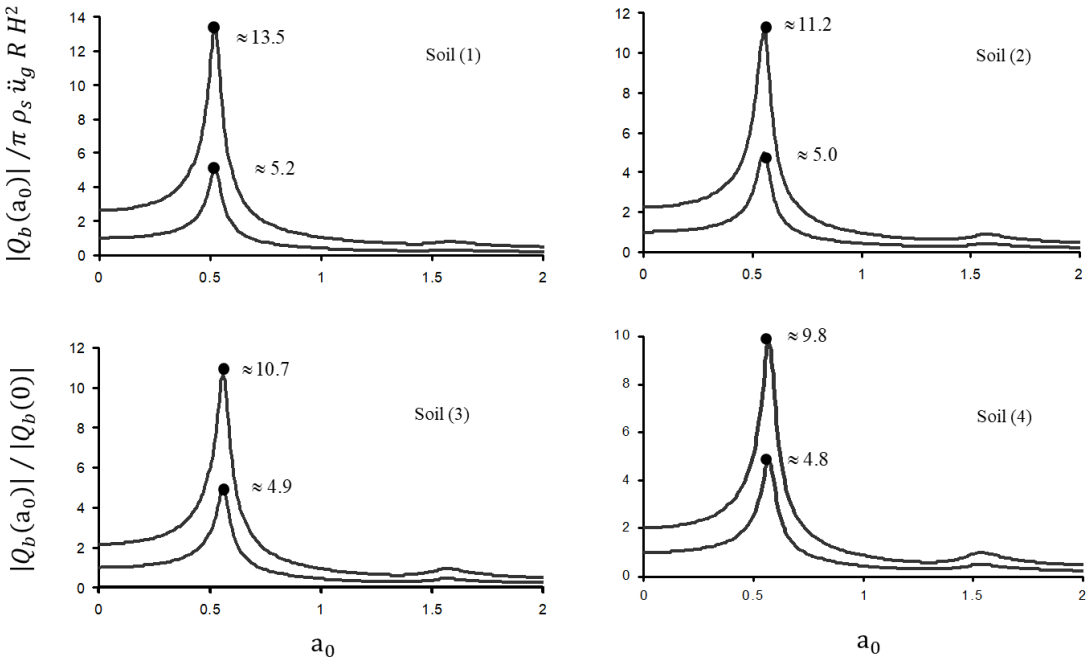

Figure 10. Variation with the dimensionless frequency a_0 of the shear at the caisson base normalized by its static value (amplification factor, $Q_b/Q_{b,st}$), and the base excitation ($Q_b/\pi\rho_s\ddot{u}_g RH^2$).

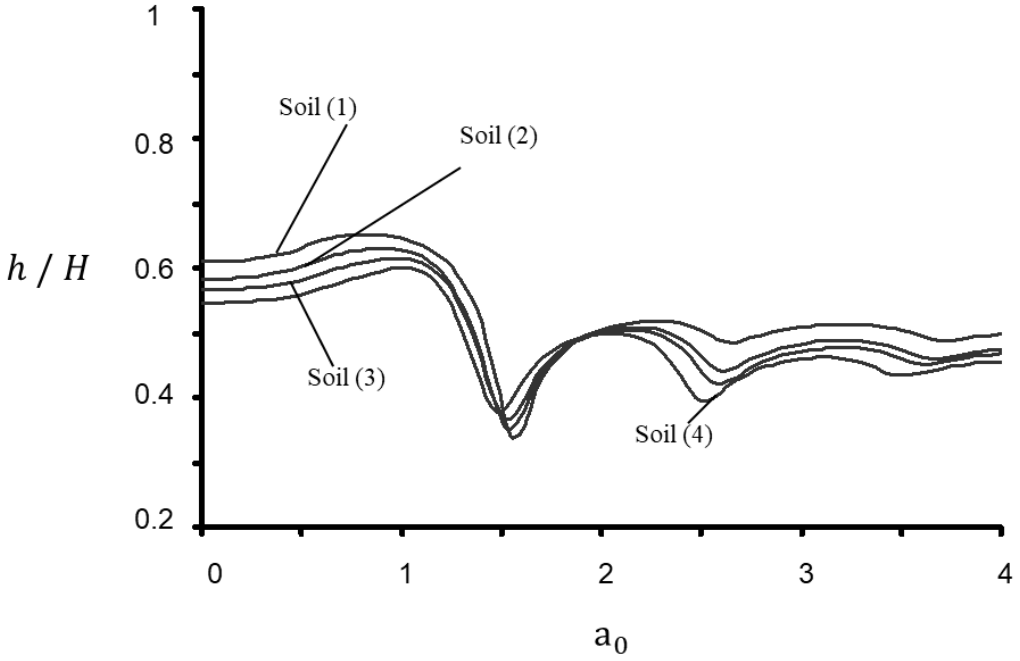

Figure 11. Variation with dimensionless frequency ratio a_0 of the normalised height of application h/H of the resultant dynamic horizontal force acting on the caisson for $H/R = 3$.

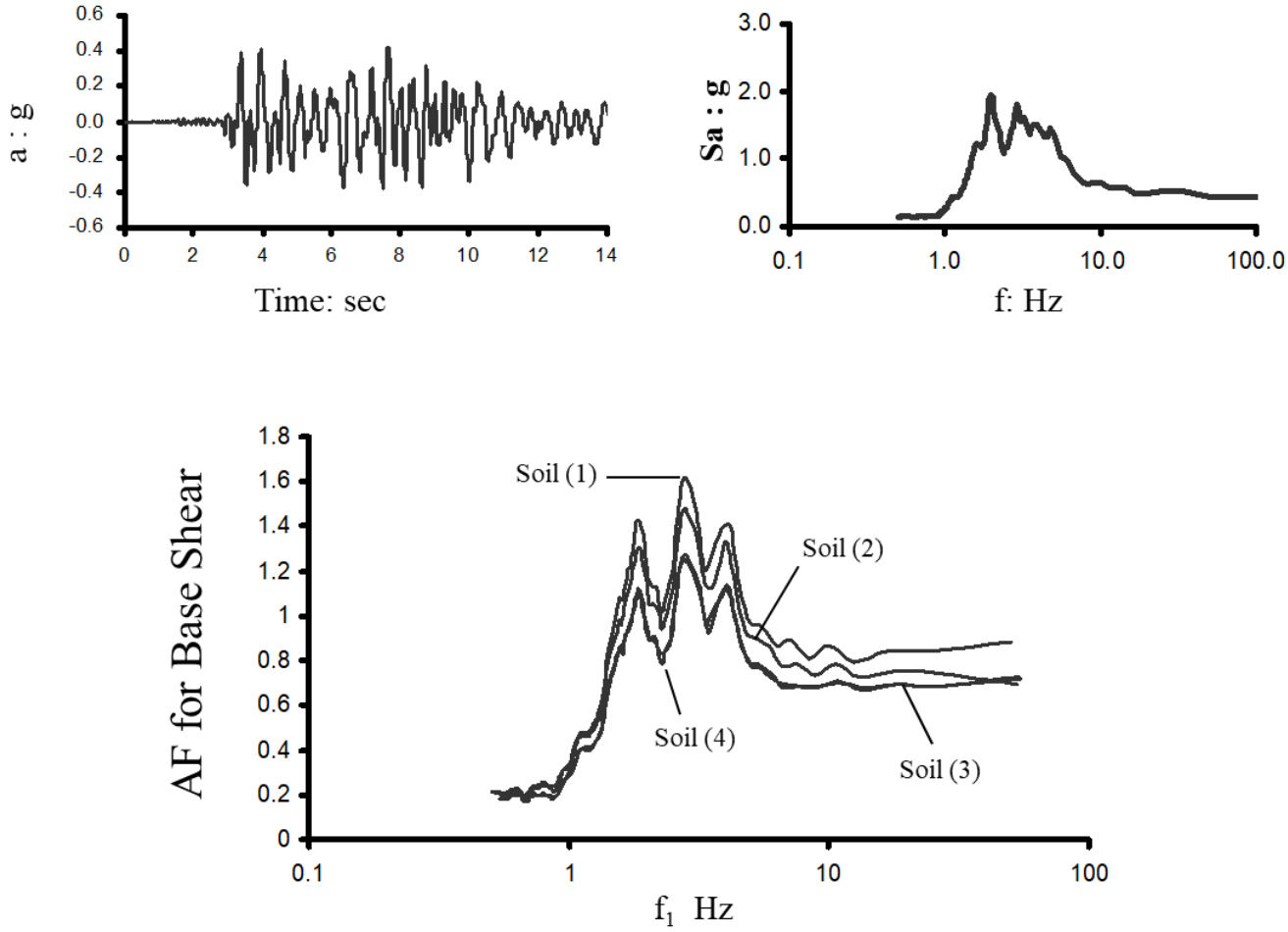

Figure 12. Amplification factor response spectra for the base shear of a caisson with $H/R = 3$, subjected to real ground motion recorded during the 6.4 magnitude earthquake in Lefkada, Greece in 2003.

Table 1. Dimensionless *m*-th natural frequencies for the different soil inhomogeneity profiles.

	Soil (1)	Soil (2)	Soil (3)	Soil (4)
$\omega_1 \mathrm{H}/\overline{V_s}$	1.57	1.65	1.68	1.71
$\omega_2 \mathrm{H}/\overline{V_s}$	4.70	4.68	4.68	4.59
$\omega_3 \mathrm{H}/\overline{V_s}$	7.83	7.77	7.71	7.47